 FDMP, vol.3, no.3, pp.265-285, 2007

Interface Deformation and Convective Transport in Horizontal Differentially Heated Air-Oil Layers

Srikrishna Sahu[1], **K. Muralidhar**[1] **and P.K. Panigrahi**[1]

Abstract: Convection in a differentially heated cavity partly filled with silicone oil has been experimentally studied. The air-oil layers are subjected to a temperature difference in the vertical direction, with the lower wall being heated with respect to the top. The overall geometry is that of an enclosed cavity that is octagonal in plan. Heights of oil layers considered for experiments correspond to 30, 50, and 70% of the vertical cavity dimension. Measurements have been carried out using a shadowgraph technique. A limited number of interferograms have also been recorded. The shadowgraph technique has been validated against interferograms under identical experimental conditions. The temperature fields in silicone oil along with the deformation of the interface have been obtained from measurements. The thrust of the study is on establishing the relationship between the interface deformation and the local heat flux, the latter measured at the interface as well as the lower hot wall. The correlation has been examined under steady as well as unsteady conditions. Nusselt number distribution over the entire air-oil interface has been determined using principles of tomography. For this purpose, the thermal field in the cavity has been mapped at four angles, namely 0, 45, 90 and 135°. When the cavity is filled up to 30 and 50% of its height with silicone oil, the Nusselt number distribution at the interface is seen to correlate directly with interface deformation. This result is seen in the instantaneous as well as the time-averaged shadowgraph images. The correlation is reversed for the lower heated wall. No interface deformation was recorded for a cavity 70% filled with silicone oil, even when the overall temperature difference was quite high.

[1] Department of Mechanical Engineering, Indian Institute of Technology Kanpur,Kanpur 208 016 UP (India).

Keyword: Convection, buoyancy, interface deformation, shadowgraph, tomography, Nusselt number.

Nomenclature

f	Fractional cavity height to which oil is filled	
g	acceleration due to gravity	$\mathrm{m.s}^{-2}$
W	width of the optical window	m
H	height of the cavity	m
I	light intensity distribution (in integer units $0 < I < 255$)	
L	length of the test cell in the optical viewing direction	m
k	thermal conductivity	$\mathrm{W{\cdot}m^{-1}{\cdot}K^{-1}}$
n	refractive index ; n_a is refractive index of air	
Nu	Local Nusselt number with gradient evaluated at the hot wall and the interface, $= -f\frac{H}{\Delta T}\frac{\partial T}{\partial y}$	
Pr	Prandtl number, $= \nu/\alpha$	
Ra	Rayleigh number, $g\beta\Delta T f^3 H^3/\nu\alpha$	
Ma	Marangoni number, $(d\sigma/dT)\Delta T H/\mu\alpha$	
σ	Surface tension	N/m
T	temperature	K
T_{hot}	temperature of the bottom hot wall	K
T_{cold}	temperature of the top cold wall	K
T_I	interface temperature	K
x	non-dimensional horizontal coordinate scaled by W	

Z_{sc}	the distance traveled by light from the point where it emerges out of the test cell to the screen where the image is captured	m
ΔT	temperature difference across the cavity, = $(T_{hot} - T_{cold})$	K
α	thermal diffusivity of silicone oil	m^2s^{-1}
β	volumetric expansion coefficient	K^{-1}
ν	kinematic viscosity of silicone oil	m^2s^{-1}

1 Introduction

Two-layer convection refers to flow patterns that appear in confined superposed fluid layers subjected to a temperature difference in the vertical direction. The two layers can be a combination of a gas and a liquid or two immiscible liquids. The layers are confined between two rigid horizontal surfaces, one heated from below and the other cooled from above. Such configurations arise in many applications including crystal growth, melt convection in weld pools and stratified water bodies such as solar ponds.

In contrast to single-layer Rayleigh-Benard convection, the simple act of adding a second layer of immiscible fluid to the system opens up a vast parameter space that can be explored. The complexity of two-layer convection is related to the facts that flow and heat transfer depend on parameters other than Rayleigh and Prandtl numbers of each fluid layer. These include the heights of the fluid layers and the fluid parameter ratios such as thermal conductivity, thermal expansion coefficient, and viscosity (Renardy and Stoltz, 2000). The main difference between one and two layer convection is the formation of an interface. With a liquid-gas combination, the interface is a free surface that may give rise to surface tension driven convection along with the buoyancy-driven. Thus, under certain conditions, interfacial tension and surface tension gradients can play important roles in determining transport phenomena.

An important feature in two-layer convection is the coupling mechanism of the flow fields in each layer across the interface. Two distinct modes of coupling between the fluid phases are possible. These are thermal (TC) and mechanical coupling (MC) respectively. In thermal coupling, the recirculation patterns in individual layers are driven by temperature difference across each of them. Thus, the hot upward flow in one layer could be above (or below) the hot upward flow in the other layer. In mechanical coupling the circulation in one layer drives that in the other by the mechanism of viscosity. Thus the two rolls are oppositely oriented and the no-slip condition is enforced at the interface. A situation is possible when the system oscillates between these two states at the onset of convection.

Convection in superposed fluid layers has been the subject of numerous experimental and theoretical investigations over the past two decades. Zhao *et al*. (1995) predicted that an indicator of what occurs in bi-layer convection could be inferred from the fluid interface instead of convection in the bulk. Four possible interface structures were realized and each one could be used to indicate the driving force of convection. Golovin *et al.* (1995) analytically studied pattern formation in a gas-liquid system with a deformable interface when the flow is Marangoni-driven. Prakash *et al.* (1997) reported experiments and numerical simulation for flow and thermal fields in the post-stability regime of two-layer convection. A rectangular cavity was considered for analysis. Andereck *et al*. (1998) reported time-dependent convection patterns in the two-layer Rayleigh-Benard system. Experiments were performed with shadowgraph and schlieren imaging techniques. In confined systems, the time dependent state was found to oscillate between MC and TC. In extended systems it was seen to manifest itself as a traveling wave that is neither precisely TC nor MC. Johnson *et al*. (1999) studied the effect of container geometry on flow patterns that form near the onset of interfacial tension-driven convection and the effect of air height on pattern formation. The numerical analysis involved solving linearized Boussinesq equations with the Chebyshev spectral-tau method. The analysis provided

the value of the critical temperature difference needed to drive convection as well the associated flow patterns. Flow visualization was carried out by an infrared camera that measured temperature distribution at the gas-liquid interface. Calculations were seen to be in good agreement with the experiments. Lebon *et al.* (2001) conducted linear stability analysis of natural thermo-convection in a two-layer system formed by a liquid and an upper immiscible gas layer. It was shown that the motion inside the gas phase could be disregarded provided its thickness was smaller than the thickness of the liquid layer. Punjabi *et al.* (2004) reported an interferometric study of convection in superposed layers of air, water, and silicone oil in the post-critical range of Rayleigh numbers. The temperature field was recorded using the Mach-Zehnder interferometer. The deformation of the fluid-fluid interface was seen to be uniformly small in all experiments. The fluid layers were found to be predominantly thermally coupled over the range of parameters studied.

The competing influences of buoyancy and surface tension under different heating conditions have been numerically studied by Lappa (2005). Closed and open parallelepiped as well as cubical containers filled with molten silicon (Pr = 0.01) were considered. Using non-linear balance equations through multiprocessor computations, stable and unstable flow fields were obtained. Three-dimensional symmetry patterns pertaining to various types of convective mechanisms (pure buoyancy, pure Marangoni and possible mixed states) under different heating conditions (horizontal or vertical temperature gradients) were illustrated. Mosaad *et al.* (2005) reported simulation of a conjugate convection problem. Here, free and forced convection boundary layers on a vertical plate were studied in addition to heat conduction across the plate. The authors estimated the mean conjugate Nusselt number over the entire plate as a function of controlling parameters. Punjabi *et al.* (2006) experimentally investigated buoyant convection in a differentially heated air-water system in a rectangular cavity using laser-interferometry. Experiments were performed with different layer thicknesses and temperature differences across the cavity. The aim of the study was towards understanding the influence of Rayleigh number on the steady thermal field, and flow coupling mechanisms between the layers. The two layers were seen to remain thermally coupled at lower Rayleigh numbers. Mechanical and thermal coupling both became significant at higher Rayleigh numbers.

A survey shows that critical points of transition, possibility of time dependent patterns at the onset of convection, oscillatory instabilities and pattern formation have been addressed in the literature. Thermal fields away from the onset of convection have not been characterized. Issues such as the origin and consequences of interface deformation and its effect on heat flux and temperature distribution over the interface have not been addressed. Against this background, the present work is concerned with gas-oil convection driven primarily by buoyancy with a focus on interfacial temperature and fluxes.

The specific objectives of the present work are to (a) visualize the convective flow patterns in silicone oil from interferograms and shadowgraph images at various oil-air height ratios and imposed temperature differences, (b) relate the deformation of the interface with the local heat flux distribution, (c) implement a tomography algorithm to obtain interfacial heat fluxes and their variation over the entire interface.

2 Apparatus and Instrumentation

A schematic drawing of the test cell used to study convection in air-oil layers is shown in Figure 1. It consists of three sections, namely the top tank, the test section and the bottom tank. The test section is octagonal in plan, has a nominal diameter of 130.6 mm and a height of 50 mm. The plan view approximates a circular cavity. The fluid layers are confined by two copper plates above and below. The octagonal cavity is essentially made of optical windows, 50 mm square and 3 mm thick, with 8 of them forming the octagon in plan. The windows are essential in the present work since they allow viewing of the thermal fields at parallel incidence and at various angles. For the octagonal geometry adopted for the experimental apparatus,

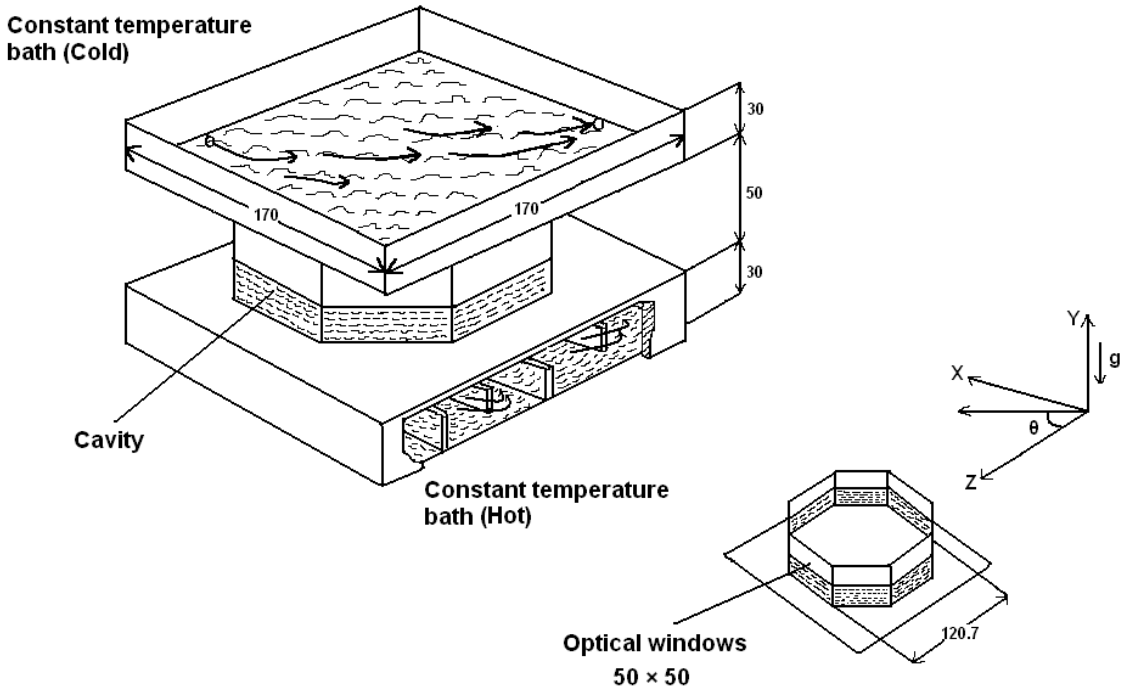

Figure 1: Schematic diagram of the octagonal test cell. (All dimensions are in mm)

view angles of 0, 45, 90, and 135˚ are possible. Both horizontal surfaces have been maintained at their respective temperatures to within ±0.1 K, the temperature control specification of the constant temperature baths.

For temperature field measurement in the fluid medium, a Mach–Zehnder interferometer has been employed. The optical layout of the interferometer is shown in Figure 2. It uses a 60 mW He–Ne laser and 150 mm diameter optics. Interferograms have been recorded using a CCD camera (PULNIX) that has a 512×512 pixel resolution. The camera is interfaced to a PC through an 8-bit A/D card which digitizes the light intensity levels over the range of 0–255. Image acquisition is at video rates (25 images·s^{-1}). The shadowgraph images have been recorded using the interferometer by blocking the reference beam. For a cavity temperature difference greater than about 4˚C, refraction errors were large and the interferograms could not be quantitatively evaluated. The shadowgraph images have been recorded in these experiments to determine the temperature field. The experimental set-up and the optical measurement procedure are similar to those described by Punjabi *et al.* (2004).

Experiments were conducted in the following manner. Silicone oil, air and the entire apparatus comprising the test cell and the compensation chamber were initially maintained at room temperature. Hot water was circulated in the lower tank to create the required temperature difference. The lower boundary attained the hot water temperature within a few minutes while the convective field evolved over a period of 4-6 hours. At the end of this time period, either a purely steady or a marginally oscillatory temperature field was realized. A long image sequence was then recorded using the CCD camera.

Direct imaging of the air-oil interface showed no visible deformation. Even under large temperature differences, the interface deformation was well-within a fraction of a millimeter, thus yielding negligible values for the interface curvature. Hence, surface tension effects can be expected to be quite small in the present work. In addition, interferometry showed isotherms to be nearly parallel to the interface, thus making it practically a constant temperature boundary. Accordingly, temperature gradients along the inter-

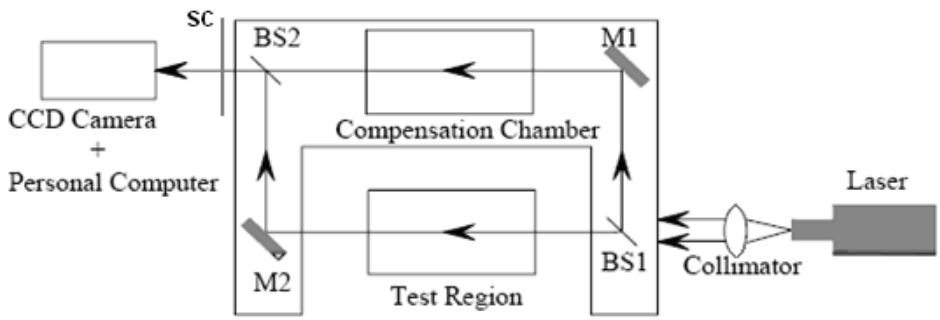

Figure 2: Schematic diagram of the Mach-Zehnder interferometer. M-Mirror, BS-Beam splitter, SC-Screen, LS-Laser source, C-CCD camera.

face were small, resulting in small Marangoni numbers (Section 5.7). The flow patterns observed in the present work can be taken to arise from a combination of viscosity, buoyancy, and inertia.

3 Data Analysis

The details of interferogram analysis have been discussed by Goldstein (1996). Fringe analysis for two-layer convection is discussed by Punjabi *et al.* (2004) and is not repeated. Data analysis using the shadowgraph images and estimation of the interface temperature using an energy balance approach are discussed in the following sections.

3.1 Shadowgraph

If the temperature difference across the fluid layer is high, three factors restrict the utility of interferometry. These are: (a) linearity of the relationship between density and temperature, (b) linearity of the relationship between density and refractive index, and (c) beam deflection due to refractive index gradients. These factors are significant when large temperature gradients appear in the flow field and complicate the data reduction process. Under these conditions, interferometry is more of a qualitative tool. However, fringes continue to form and images can be used for flow visualization. In the present work, interface deformation was seen under conditions of high temperature differences across the cavity. Hence, experiments with a visible interface movement have been analyzed using the shadowgraph technique. Other experiments in which the overall temperature difference is small have been analyzed using interferometry.

Shadowgraph is a single beam technique where the change in light intensity with beam divergence is utilized to estimate temperature distribution in the fluid medium. Quantitatively, the intensity distribution is interpreted as the Laplacian of the temperature field; this is in contrast to interferometry where direct measurement of temperature is possible. Specifically the shadowgraph measures the variation of the second derivative of refractive index along coordinates normal to the direction of propagation of the light beam (Settles, 2001).

In the shadowgraph technique, the change in the intensity field ΔI relative to the background intensity distribution I can be related to the refractive index field directly as (Goldstein, 1996; Settles, 2001):

$$\frac{\Delta I}{I} = -\frac{Z_{sc}}{n_a}\int_0^L \left(\frac{\partial^2 T}{\partial x^2} + \frac{\partial^2 T}{\partial y^2}\right)\frac{dn}{dT}dz \qquad (1)$$

Here Z_{sc} is the distance traveled by light, from the point where it emerges out of the test cell to the screen where the image is recorded, n_a is refractive index of the ambient and dn/dT is the change in refractive index with respect to temperature in the fluid medium under consideration. In Equation 1, x and y denote coordinates perpendicular to z, the direction of propagation of light. In addition, y is the vertical direction along which the temperature difference is applied. It is assumed at this point that temperature changes principally in the y direction and changes with respect to $x$are of secondary consequence. With this assumption,

Equation 1 can be written as

$$\frac{\Delta I}{I} = -\left(\frac{Z_{sc}L}{n_a}\right)\left(\frac{dn}{dT}\right)\frac{\partial^2 \overline{T}}{\partial y^2} \tag{2}$$

Here $\overline{T}$ is the path averaged temperature in the viewing direction (within the cavity) and L is the length of the test section in the z direction. The second derivative of temperature in the y direction can now be expressed as

$$\frac{\partial^2 \overline{T}}{\partial y^2} = -\frac{\Delta I/I}{\left(\frac{Z_{sc}L}{n_a}\right)\left(\frac{dn}{dT}\right)} \tag{3}$$

The partial derivative symbol on the left hand side of Equation 3 is retained because temperature can be a function of time as well. Since optical methods are inertia-free, Equation 3 is applicable for each instant of time. Integration of Equation 3 with suitable boundary conditions is discussed in Section 4.

3.2 *Determination of interface temperature from correlations*

The knowledge of the average interface temperature is useful in determining the equivalent Rayleigh number driving convection in each of the fluid layers. It can also be used for data analysis of temperature from interferograms and shadowgraph images. Here, steady state is assumed and the principle of conservation of energy is applied to estimate the average interface temperature. With T_I as the interface temperature, we have

$$h_1(T_h - T_I)A = h_2(T_I - T_c)A$$

Here h_1 and h_2 are the respective heat transfer coefficients in the two fluid layers. In terms of the respective Nusselt numbers, the heat transfer coefficients in air and oil can be estimated as $h_1 = \mathrm{Nu}_1 k_1/d_1$ and $h_2 = \mathrm{Nu}_2 k_2/d_2$. Quantities d_1 and d_2 are the characteristic dimensions of the fluid layers 1 and 2 in the vertical direction. With f representing the fraction up to which the cavity is filled with oil, these dimensions can be written as $f \times H$ and $(1-f)H$ respectively. Hence, the energy balance equation can be expressed as:

$$\frac{\mathrm{Nu}_1 k_1 (T_h - T_I)}{f} = \frac{\mathrm{Nu}_2 k_2 (T_I - T_c)}{(1-f)} \tag{4}$$

The average Nusselt number for individual fluids can be obtained from the single fluid correlations given by Gebhart *et al.* (1988). The correlations are based on independently conducted experiments on a single fluid in a horizontal differentially heated cavity. They do not explicitly contain the aspect ratio as a parameter. The correlations have a large uncertainty band of around $\pm 20\%$. Differences are also to be expected since in the present experiments, the single fluid layer is confined between top and bottom boundaries with rigid no slip walls, while in the two fluid configuration, one of the boundaries is a fluid interface.

Equation 4 is evaluated as follows. The interface temperature (T_I) is first assumed to be a value between T_h and T_c. The Rayleigh numbers corresponding to each fluid layer are then calculated. The average Nusselt numbers are calculated from the heat transfer correlations. The interface temperature T_I is re-calculated from Equation 4. The above procedure is repeated till convergence in the interface temperature is reached.

4 Validation of the Image Analysis Procedure

The measurement procedure using interferometry has been validated in the previous work of the authors (Mishra *et al.*, 1999; Punjabi *et al.*, 2004) and is not repeated here. The validation of the shadowgraph technique against interferometry is presented below.

Once the shadowgraph image is recorded, Equation 3 yields the second derivative of temperature $\partial^2 T/\partial^2 y$ at each pixel along any vertical column. Integration of Equation 3 requires the knowledge of two boundary conditions to obtain the vertical temperature distribution. In the experiments of the present work, only one boundary condition, namely the lower wall temperature is clearly known. No explicit information at the oil-air interface is *a priori* available. Three possible boundary conditions at the interface (a-c) are proposed here.

a) From Equation 4, the interface temperature is calculated. The entire interface is taken to be at this temperature. Thus we have the first set

of boundary conditions:

$$\begin{aligned} &\text{At lower wall, } T = T_{hot};\\ &\text{at interface, } T = T_{\text{interface}} \end{aligned} \tag{5}$$

b) Here, the interfacial heat flux in silicone oil is determined using the Nusselt number correlation for the portion of the cavity containing air. Hence

$$-k_{oil}(\partial T/\partial y) = h_{air}(T_{hot} - T_I)$$

Heat transfer coefficient h_{air} is obtained using the single fluid correlation in terms of Nusselt number. From the above equation the temperature gradient at the interface can be obtained. The second set of boundary conditions is written as:

$$\begin{aligned} &\text{At lower wall, } T_{wall} = T_{hot};\\ &\text{at interface, } \partial T/\partial y = \text{given} \end{aligned} \tag{6}$$

c) The single fluid correlation can also be used in silicone oil to determine the average heat flux at the lower wall. Thus, the third set of boundary conditions is written as:

$$\text{At lower wall, } T_{wall} = T_{hot} \text{ and } \partial T/\partial y = \text{given} \tag{7}$$

These three boundary conditions are identified as Shadowgraph-1, Shadowgraph-2 and Shadowgraph-3 respectively in the accompanying figures.

A detailed comparison of temperature profiles in silicone oil determined from shadowgraph as well as interferometric analysis is given in Figure 3. The overall temperature difference ΔT in the experiments is 2.4 K. The fractional temperature drop in silicone oil is less than 1 K. Three layer heights of silicone oil are considered. The shadowgraph images have been evaluated with the three boundary conditions (Equations 5-7) presented above. Image analysis using Shadowgraph-1 (Equation 5) shows the best match with interferograms. Interferometry and shadowgraph match identically at the lower wall where the wall temperature is prescribed in the analysis of both images. The fact that Equation 5 predicts a temperature at the interface close to that of interferometry validates the shadowgraph analysis procedure. The overall success of Equation 5 is also to be expected since the interferograms indeed show the interface to be nearly an isotherm. There are, however, differences in terms of temperature gradients, particularly near the wall and the interface. Here, interferometry is possibly inaccurate owing to refraction errors (Goldstein, 1996). The predictions of Shadowgraph-2 (Equation 6) are close to interferometry for the 30% filled cavity. The differences increase sharply at other oil heights. Boundary conditions given by Shadowgraph-3 (Equation 7) show the largest deviation with respect to interferometry, both in terms of gradients as well as temperature. This is expected because both boundary conditions are applied at the same location. Here, Equation 3 is reduced to an initial value problem that is numerically ill-posed.

Based on the discussion above, shadowgraph images have been evaluated using Equation 3 and boundary conditions given by Equation 5. For small temperature differences, temperature profiles have been derived using interferograms as well.

5 Results and Discussion

For the parameters considered in the experiments, specifically cavity temperature difference and cavity height, the temperature drop in air is greater than that in silicone oil owing to the high thermal conductivity of the latter. The temperature changes per fringe shift in air and silicone oil are 5.65 and 0.012 K respectively. Thus, for the range of applied temperature difference considered, practically no fringes in air were seen; in silicone oil dense fringes were realized. In the octagonal cavity the roll structures are expected to form concentric rings (Velarde and Normand, 1980). The fringes are contours of constant depth averaged temperature and arrange themselves to form a Ω-pattern (Punjabi *et al.*, 2004). The full thermal field in silicone oil is seen as a collection of omega and inverse-omega contours interlinked with one another.

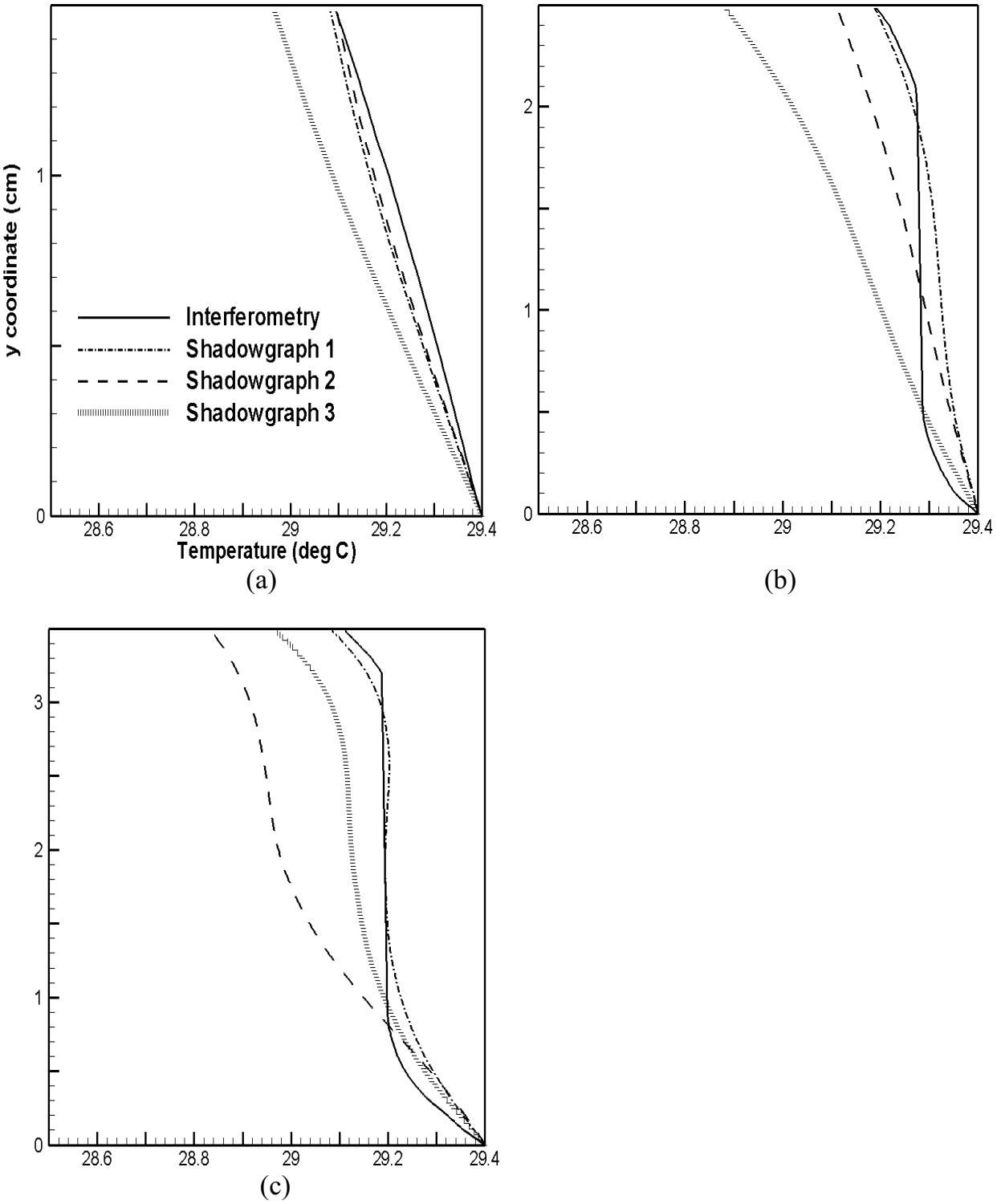

Figure 3: Comparison of temperature profiles obtained through shadowgraph evaluation as against interferometry at a cavity temperature difference of $\Delta T = 2.4$ K. Oil layer heights in each experiment are (a) 30%, (b) 50%, and (c) 70%

In the present work three oil layer heights (30, 50 and 70% of the vertical cavity dimension) have been considered. For each oil level, four temperature differences (ΔT = 0.4, 2.4, 5, 10 K) across the cavity drive the convective field. For overall temperature differences of 0.4 and 2.4 K, the experimental data obtained are in the form of interferograms. For larger temperature differences of 5 and 10 K, shadowgraphs have been evaluated to obtain the vertical temperature profiles.

5.1 Effect of temperature difference across the cavity

Figure 4 shows interferograms and shadowgraph images obtained for various temperature differences across the cavity when it is half-filled with silicone oil. As the overall temperature difference across the cavity increases, the temperature change across silicone oil increases, though a greater reduction in temperature takes place in air. Hence, there is a continuous increase in Rayleigh number for each fluid with temperature difference across the cavity. With an increase in Rayleigh number, Figure 4 shows that the number of fringes increases. The fringe density near the interface also increases indicating an increase in the heat flux at the air-oil interface. The fringes are practically aligned with the interface. Thus, the interface tends to become an isotherm. For this reason, convection driven by surface tension gradients along the interface is expected to be small in the present work. The comparison is against the contribution of buoyancy that scales with the cavity temperature difference. The high fringe density and consequently, the large interfacial flux suggests that air and oil are thermally coupled, the convection in each fluid layer being driven by their respective temperature difference. The sum of the two temperature differences is equal to that applied across the cavity. For an increase in temperature difference, Figure 4 shows that the center of the Ω-shaped fringe moves away from the interface and towards the lower wall. Thus, there is a reduction in the size of the recirculation roll at higher temperature differences.

Though not noticeable at lower temperature differences, Figure 4 shows visible interface deformation at a temperature difference of 10 K.

5.2 Effect of layer height

Figure 5 presents data on the effect of layer height on the convection pattern in silicone oil. The temperature profiles along the mid-plane of the cavity are also shown. Layer heights of 30, 50 and 70% with respect to the vertical cavity dimension are considered. The overall temperature difference across the cavity is 2.4 K in these experiments. For a given cavity temperature difference, the temperature drop across the oil layer is expected to increase with layer height since the air layer continuously becomes thinner. Consequently, a reduction in the interface temperature with an increase in the layer height of oil is to be expected. As the layer height increases from 30 to 50%, the temperature profiles show that the interface temperature first increases and subsequently decreases for the 70% experiment. The temperature change is quite small ($\sim$0.1°C) but could be recorded through the interferograms. These observations can be explained as follows. For the 30% layer height, heat transfer takes place by conduction and fluid velocities are quite small. The temperature profile in the oil layer is linear. With 50% layer height, convection is initiated in the oil layer. Temperature gradients are large near the wall and near the interface, while it is practically a constant (close to zero) in the middle. The absence of a temperature drop in the core of the oil layer contributes to a slight increase in the interface temperature. At 70% layer height, convection in silicone oil is quite vigorous, the air resistance is also lowered but a net reduction in the interface temperature is obtained. In general, a lowering of the interface temperature is to be expected after the onset of convection in the oil phase.

5.3 Imaging convection as a function of view angle

Figure 6 shows interferograms and shadowgraph images obtained at ΔT = 5 K for four different view angles. The cavity is filled with 50% silicone oil, leading to a Rayleigh number of 6106 and 20062 in air and oil respectively. In the in-

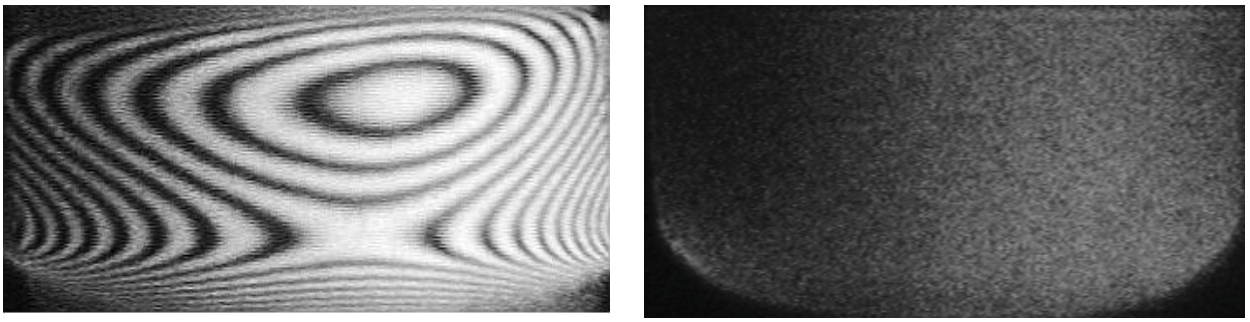

(a) $\Delta T = 0.4$ K

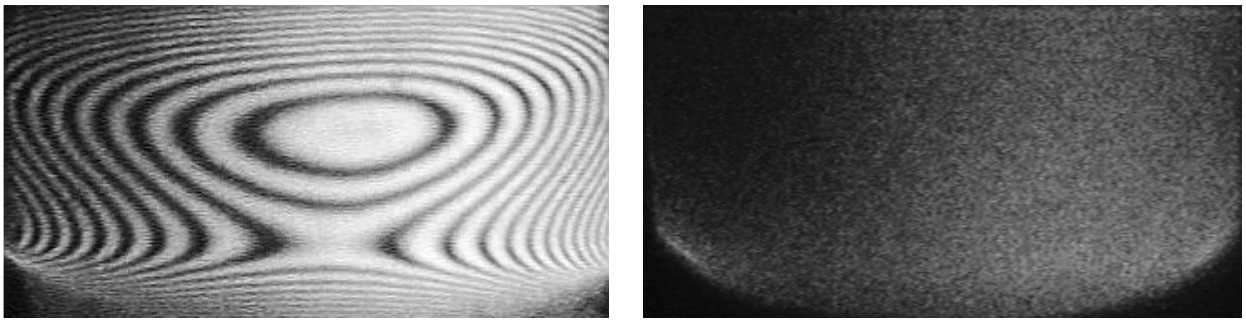

(b) $\Delta T = 2.4$ K

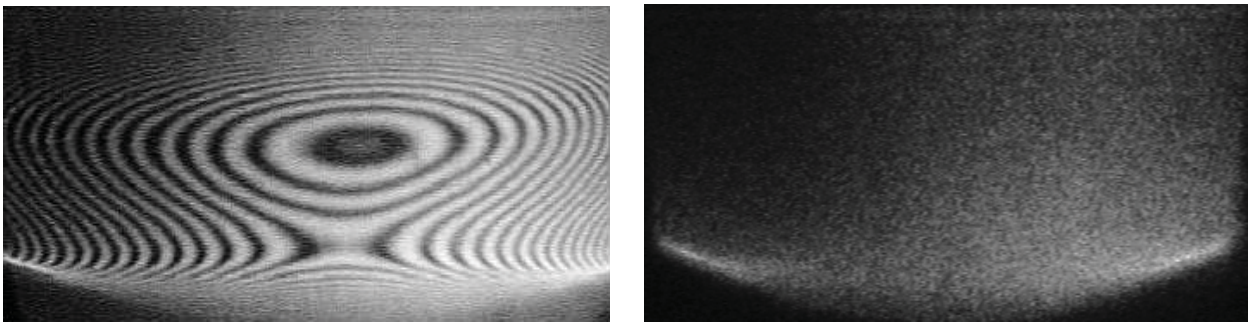

(c) $\Delta T = 5$ K

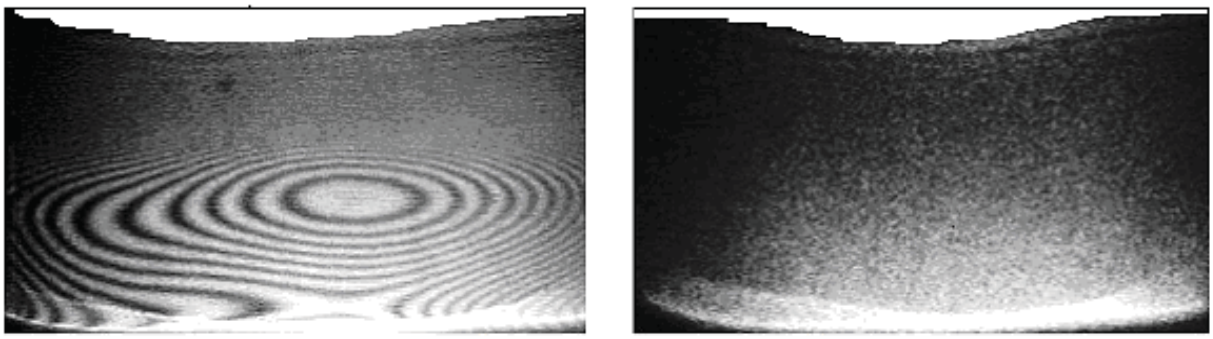

(d) $\Delta T = 10$ K

Figure 4: Interferograms and shadowgraphs that show the effect of increasing the overall temperature difference (ΔT) across the cavity which is 50% filled with silicone oil. Interface deformation is clearly seen in (d).

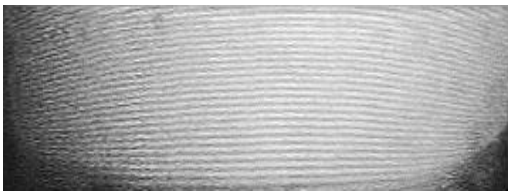

(a) 30%

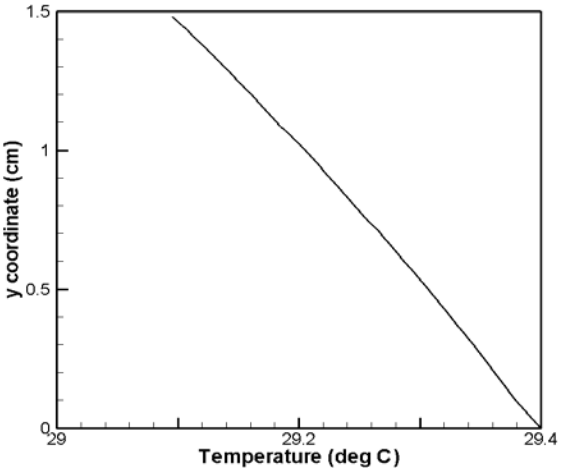

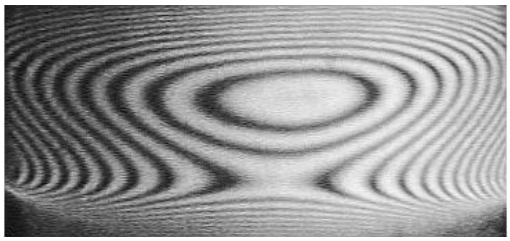

(b) 50%

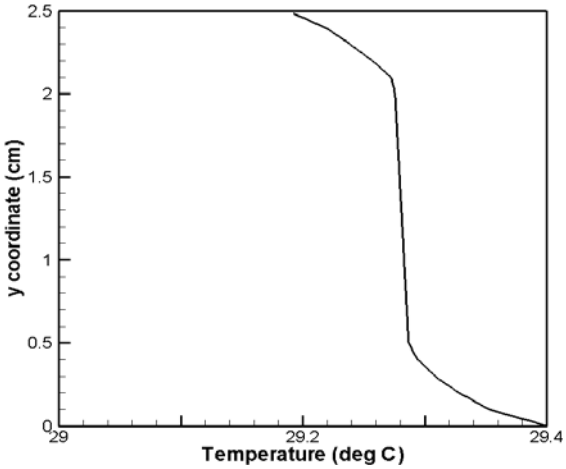

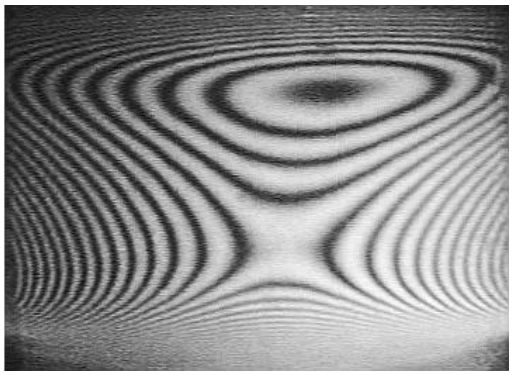

(c) 70%

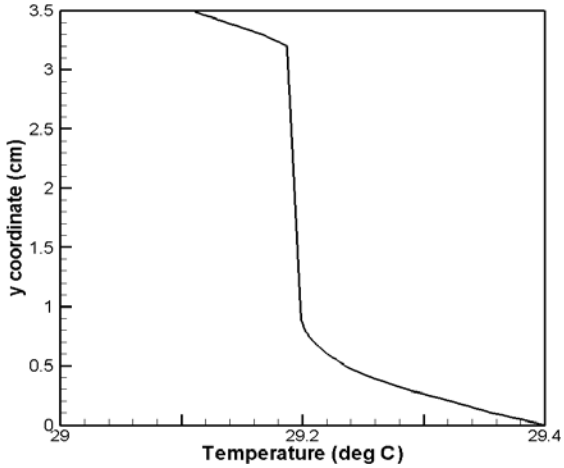

Figure 5: Effect of variation of variation of oil layer height: Interferograms and corresponding temperature profiles for cavity with three different silicone oil layer heights at $\Delta T = 2.4$ K.

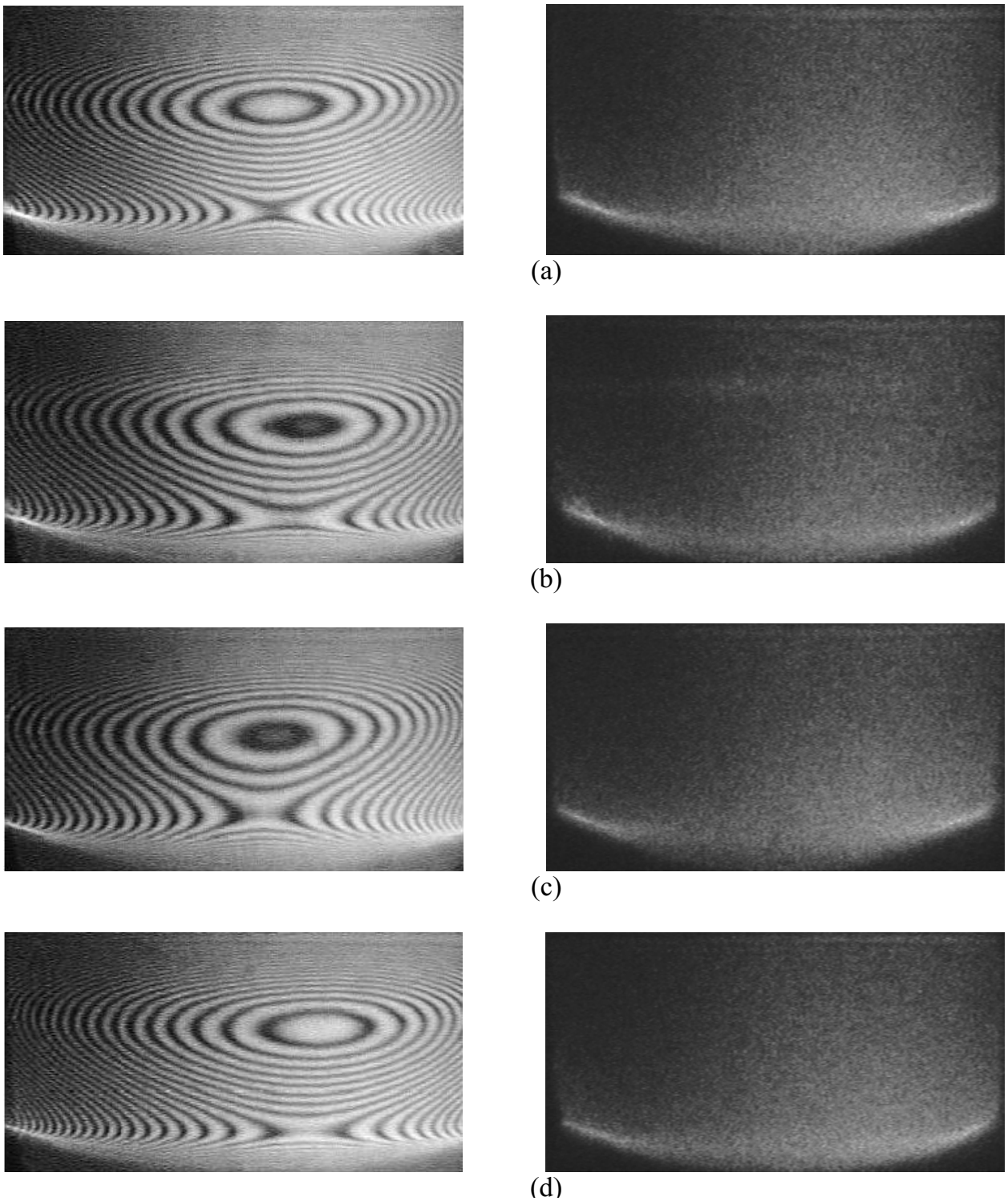

Figure 6: Interferograms and shadowgraphs for an overall temperature difference $\Delta T = 5$ K. The cavity is 50% filled with silicone oil. View angles considered are (a) 0, (b) 45, (c) 90, and (d) 135° respectively. Clear changes in light intensity were seen in shadowgraphs only at higher temperature differences.

terferograms, the fringes very near the hot wall are lost due to refraction. The lower wall in turn appears to be deformed. The interface however, appears to be quite flat. Owing to a high fringe density at the interface, interferometric analysis was not possible. Results based on shadowgraph evaluation are reported below. The interferograms show clear variation among the different view angles. The difference in the nature of variation can be ascertained from the location of the center of the Ω-shaped fringe. Thus, the convective field in silicone oil is three dimensional. Experiments of Krishnamurti (1970) in a single fluid Rayleigh-Benard system show that the convective field at Ra=20062 and Pr=11 (for silicone oil) will indeed fall in the steady three dimensional regime. The result carries over to the air-oil combination and confirms that the fluid layers are thermally coupled.

5.4 Unsteady convection with interface deformation

At low cavity temperature differences (0.4 and 2.4 K), convection is steady and the interface deformation is negligible (Figures 4-5). At higher temperature differences (=5 K), the convective field becomes three dimensional but the interface deformation continues to be insignificant (Figure 6). At very high Rayleigh numbers (corresponding to an overall temperature difference of 10 K and greater), the convective field in oil is unsteady and a significant interface deformation is seen. In addition, the interface is seen to move with time. At low oil layer heights (say 30%), the equivalent Rayleigh number is small and convection is quite weak. The corresponding interface deformation is small. At a 50% layer height, a range of convective phenomena is observed, with interface deformation becoming visible at high temperature differences. When the layer height is 70%, the roll size is large and circulation is less intense. Convection, in this respect is weakened and once again the interface deformation is diminished. For this reason, subsequent discussions focus on experiments with 50% oil-filled cavity, where a visible interface deformation was seen.

The interferogram and shadowgraph images at a particular instant of time for a cavity temperature difference ΔT of 10 K and 50% silicone oil was shown in Figure 4(d). Here, the hot and cold walls were at 29.4 K and 19.4 K respectively. At such a large temperature difference, the near wall fringes at the heated boundary are lost and some amount of image distortion takes place. The interface temperature from the energy balance approach was calculated to be 28.12 K. The corresponding Rayleigh numbers in air and oil are 12244 and 39425 respectively. The interferogram shows dense parallel fringes near air-oil interface. Thus, the interface can be considered to be at a uniform temperature even when continuously deforming with time. This observation justifies the analysis reported here based on the constant temperature interface condition.

The time sequence of interface deformation is shown in the form of shadowgraph images in Figure 7. These images were recorded with a time interval of 5 seconds. The images of Figure 7 bring out the periodicity in interface deformation with time. The full layer of silicone oil is shown, the vertical extent of the shadowgraph region being 25 mm. From Figure 7, the maximum interface deformation is estimated to be around 5 mm. The time scale of periodicity is $\tau = 20$ seconds, corresponding to a frequency of 0.05 Hz. The corresponding Fourier number $(= \alpha\tau/h^2)$ based on the half cavity height h=12.5 mm is 0.013. Here, the thermal diffusivity α of 50 cSt silicone oil is taken to be 1.05×10^{-7} m^2/s. The Fourier number quoted by Gollub and Benson (1980) is 0.25, based on their LDV studies of unsteady Rayleigh-Benard convection in the post-critical regime. Thus, interface deformation is seen to be driven by surface movement and does not scale with time-periodic convection within the bulk of the oil layer. Unsteadiness in air is also not a relevant mechanism for interface movement. In summary, Figure 7 provides evidence of surface waves even when thermal coupling between air and oil layers prevail in the unsteady convection regime.

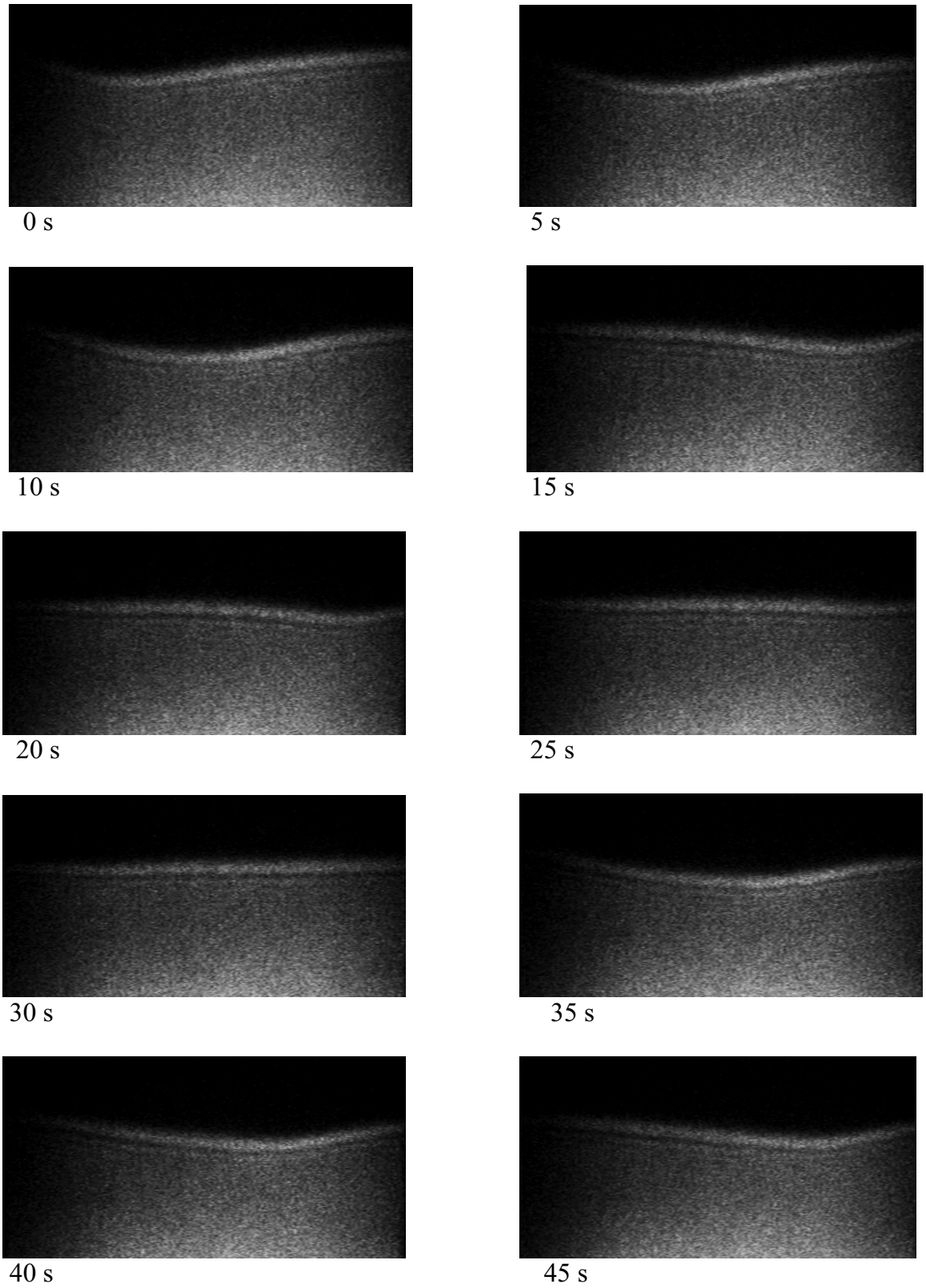

Figure 7: Sequence of shadowgraph images that show interface deformation at different time instants with an interval of 5 seconds. The cavity temperature difference is $\Delta T = 10$ K.

5.5 *Effect of interface deformation on heat flux*

In the present section, the correlation between interface deformation and the local interfacial heat flux is examined. The analysis is performed with the help of the instantaneous shadowgraph images. The interfacial flux is reported in dimensionless form and equivalently in terms of the local Nusselt number as a function of the coordinate in the positive x-direction. The Nusselt number variation along the lower heated wall is also included for comparison. Figure 8 presents the variation of Nusselt number over the interface and the lower wall along with interface deformation for 10 different time instants. Figure 9 presents the time-wise variation of Nusselt number at the interface and the heated wall at three different x-locations. The instantaneous plot with respect to the space-coordinate and the temporal variations show a strong association among interface flux, wall flux and interface deformation. From Figures 8 and 9, the following conclusions can be drawn:

1. The Nusselt number at the interface has a positive correlation with interface deformation. Thus, regions of large deformation from the mean position are also regions of high interfacial heat flux. Conversely, the downward movement of the interface also lowers the interfacial flux.

2. The correlation between interface deformation and Nusselt number is seen in instantaneous shadowgraph images as well as in the entire time sequence.

3. The wall Nusselt number negatively correlates with the interface deformation for a given streamwise position along the cavity.

The above observations can be explained in the following manner. The vertically upward movement of the interface increases its distance from the lower wall and thus increases the conduction resistance. Consequently, a reduction in heat flux is to be expected. The shadowgraph experiments reveal an opposite trend for the following reason: The crest of the interface and the point of maximum heat flux at the lower wall are both parts of a single recirculation loop created by buoyancy. The circulation pattern communicates the peak heat flux from the wall to the highest point on the interface, creating a joint maximum in displacement and Nusselt number at that location. Directly below the crest, the fluid motion is less vigorous and a minimum in the heat flux is obtained. A second factor that contributes to the positive correlation is fluid velocity. At the crest of the interface, it is expected that the x-component velocity is high, resulting in large heat fluxes across the interface. For a similar reason, the heat flux reaches a minimum below a trough in interface displacement.

The correlation between heat flux and interface displacement was observed in sequences of images recorded in experiments with an identical temperature difference. It was also to be seen in all the four view angles at which shadowgraph imaging was conducted. Experiments conducted with a large temperature difference across a cavity with 30% silicone oil revealed some interface deformation. A shadowgraph analysis of the recorded images once again showed a correlation between interface movement and the interfacial flux. For a cavity with 70% oil, the interface movement was very small and the correlation could not be ascertained.

In a numerical study, Golovin *et al.* (1995) have referred to an additional heat flux created at the moving deformable interface that originates from a surface tension gradient and interfacial deformation. A closer comparison is not possible since surface tension and its gradients are only of secondary importance to the present work (also see Section 5.7).

5.6 *Three dimensional reconstruction of Nusselt number*

The Nusselt number distribution of Section 5.5 is an average evaluated along the viewing direction. The present section is concerned with obtaining the local distribution of Nusselt number at every point over the entire interface. A similar distribution at the lower wall is also of interest. The reconstruction of Nusselt number over the interface has been accomplished by first record-

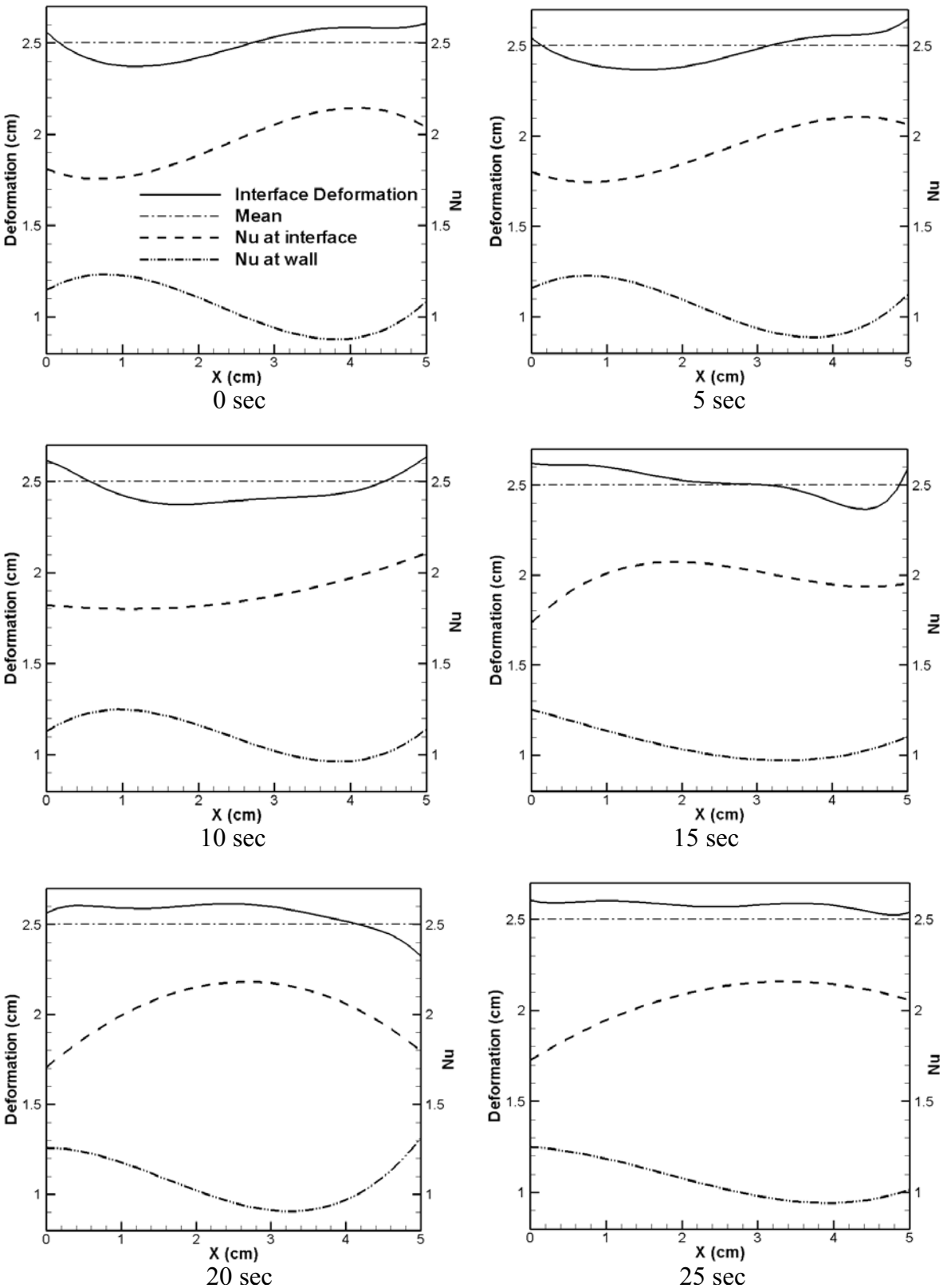

Figure 8: Interface deformation and Nusselt number variation over the interface and the lower hot wall for different time instants; $\Delta T = 10$ K. The cavity is 50% filled with silicone oil.

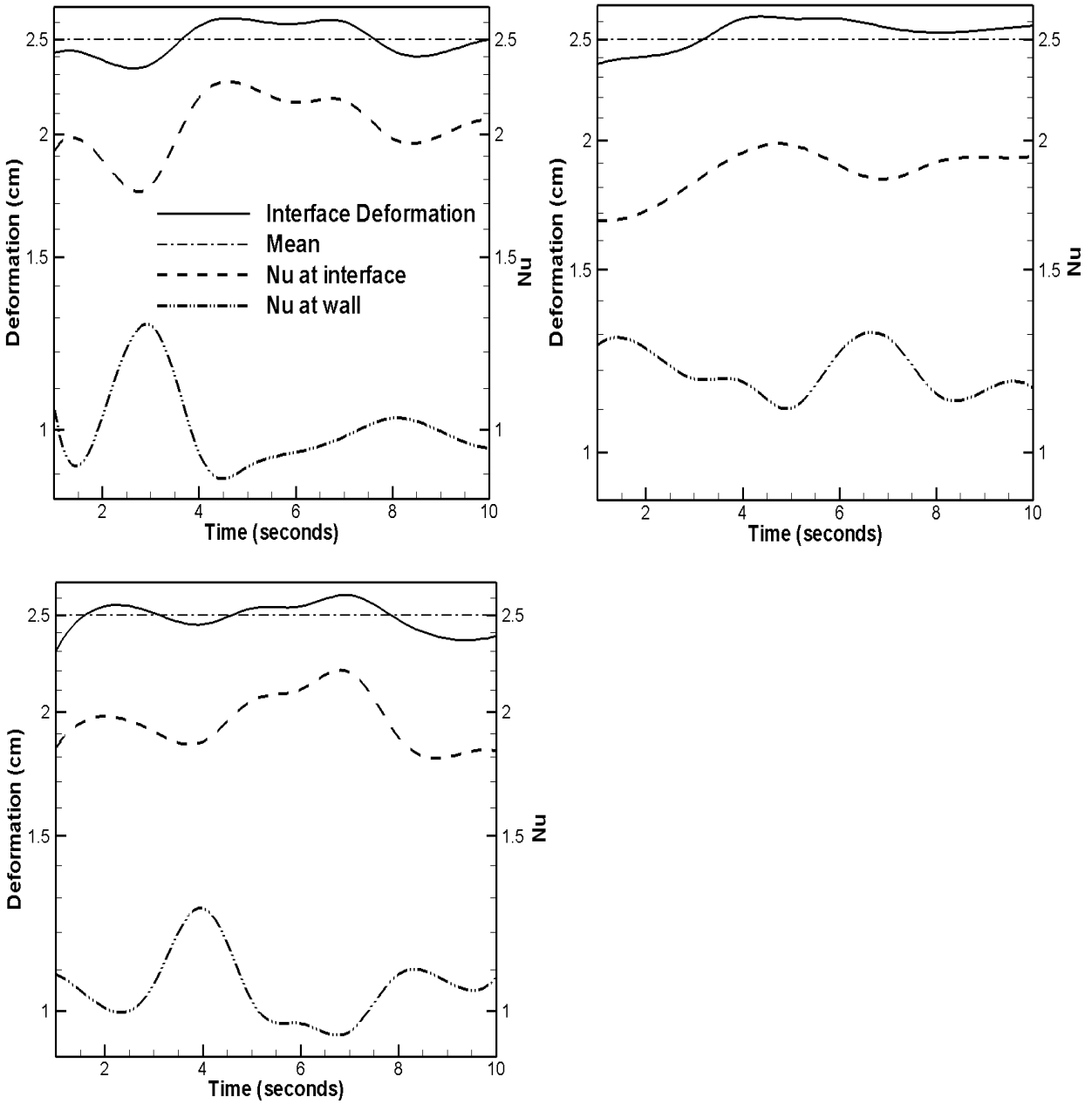

Figure 9: Temporal variation of interface deformation compared with Nusselt numbers at the interface and wall for three dimensionless x locations. (a) x = 0.25, (b) x = 0.5 and (c) x = 0.75. Overall temperature difference $\Delta T = 10$ K; The cavity is 50% filled with silicone oil.

ing shadowgraph images along four distinct view angles. Interpreting each view as a path integral (Equation 2) and applying tomographic algorithms, specifically, convolution back projection (CBP), the variation of Nusselt number over an entire surface has been obtained. Tomography can be applied in principle only for time-invariant fields (Herman, 1980; Natterer, 1986). In the present work, tomography has been applied to specific modes of convection that are in turn determined by a proper orthogonalization procedure (Jollife, 2000). The input to these calculations is a time sequence of shadowgraph images for each view angle.

Proper orthogonal decomposition (POD) is a powerful method of data analysis that converts a function of both time and space into a product of functions that depend individually on space and time. Functions of space thus obtained are the modes contained in the data set. The decomposition is performed in an optimal manner in such a way that the lowest modes contain most information about the entire time sequence. The zeroth-order mode is obtained as an average of the time sequence of shadowgraph images. In the present experiments, the time sequence of shadowgraph images are converted into modes of various orders for each view angle. It is assumed that modes of identical order for each of the viewing directions uniquely correspond to one another and hence can be used for tomography. Both POD and tomography calculations have been performed in the present work using MATLAB. The numerical procedure has been validated against simulated data where the field of the dependent variable was taken as a function of x, y and time. The errors in reconstruction were found to be less than $\pm 1\%$.

Figure 10 shows the zeroth-order Nusselt number distribution over the interface and the lower (heated) wall. Figure 10 also shows the first and the second modes of Nusselt number for the interface and the lower wall. In continuation to the discussion in Section 5.5, the interfacial Nusselt number distribution is seen to correlate positively with the interface deformation. The bright patch in the reconstructed grey-scale image of Nusselt number indicates high values of the interfacial flux. Figure 10 shows that bright regions in the central portion of the interface correspond to dark regions at the lower wall. Darker regions at the interface also correlate with brighter regions at the lower wall. These results are generalizations of the trend seen in Figures 8 and 9. The flux-deformation correlation holds for both the first and the second modes. Hence, the observations of Section 5.5 can be taken to be applicable in the space as well as time domain.

5.7 Effect of surface tension gradients

For the present set of experiments, surface tension gradient can be shown to have a negligible effect on the interface deformation. Rayleigh number (Ra) is proportional to the third power of layer height as compared to the first power dependence of Marangoni number (Ma). For deep fluid layers, buoyancy-driven convection is more prevalent, and for shallow depths, interfacial tension gradient driven convection is dominant. For all temperature differences considered in the present work, the interferograms show dense and nearly parallel fringes near the interface (Figures 4-6). This indicates that the interface behaves as an isotherm. If it is assumed that three fringes intersect the interface, one can calculate Ma for equal layer heights to be close to 9. The critical Marangoni number needed to initiate fluid motion is around 80 (Shyy *et al.*, 1996). The critical Rayleigh number for onset of convection is around 2000, while its value in experiments was in the range of 20,000-40,000. Taken together, it can be concluded that Marangoni effects are insignificant in comparison to buoyancy and do not contribute to the deformation of the interface.

6 Conclusions

Convection in a differentially heated cavity that is octagonal in plan has been investigated. The cavity was partly filled with 50 cSt grade silicone oil. Three layer thicknesses (30, 50, and 70% of the cavity height) were examined during the experiments. The overall temperature difference across the two walls ranged from 0.4 K to 10 K. The temperature fields in the oil layer were imaged by the interferometry technique for small temper-

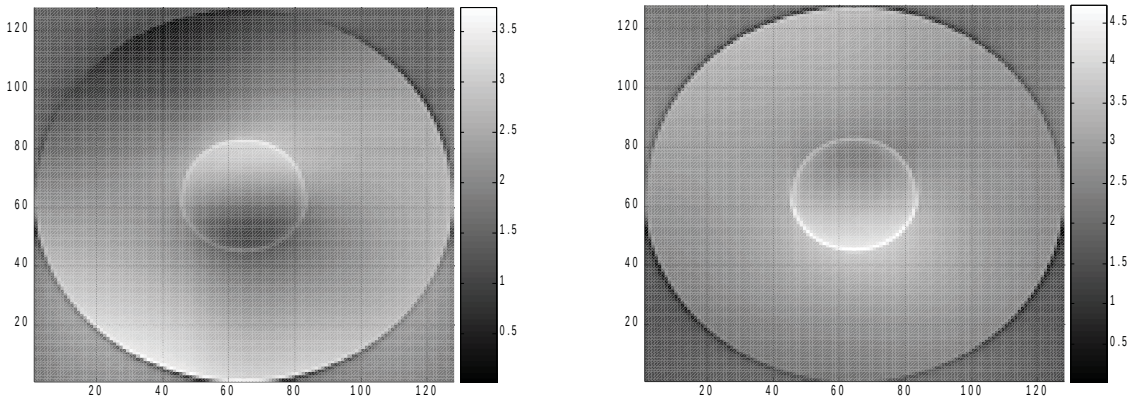

(a) Mode-0 (time-average)

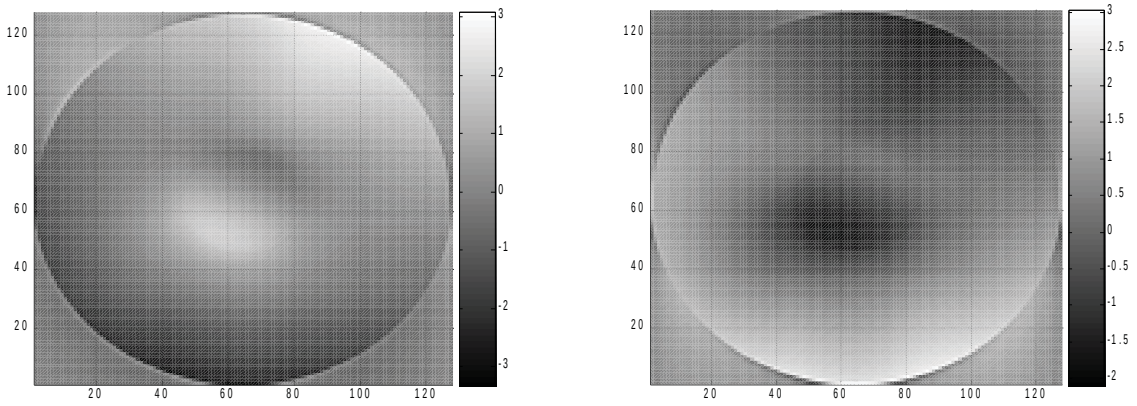

(b) Mode-1

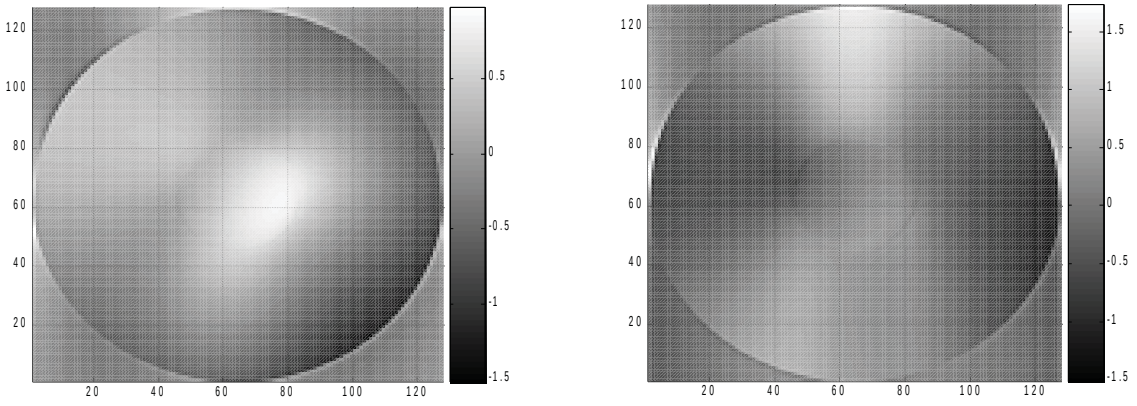

(c) Mode-2

Figure 10: (a) Time-averaged Nusselt numbers corresponding to Mode 0 at the lower wall (left) and the interface (right). (b) The first mode of Nusselt number at the wall (left) and the interface (right). (c) The second mode of Nusselt number at the wall (left) and the interface (right).

ature differences and by shadowgraph for larger temperature differences across the cavity. Major observations derived from the present study are summarized below:

1. Flow and transport in air and oil layers were seen to be controlled by their respective temperature differences. The average interface temperature was close to the value predicted by an energy balance approach that assumed buoyancy as the sole driving force. Interferometric fringes were seen to be parallel to the interface, indicating that the interface was practically at a constant temperature. Thus the fluid layers were thermally coupled for the range of parameters considered in the present work.

2. Interface deformation and unsteadiness in the thermal field were seen for an overall temperature difference of ΔT=10 K when the cavity was filled with oil up to 30 and 50% of the cavity height.

3. The interface deformation showed a positive correlation with the local interfacial flux, being large in regions of large displacement. The correlation between interface movement and the lower wall heat flux was negative. These results showed the appearance of a roll in the cavity spanning the entire oil layer.

4. Time-averaged (zeroth order) mode along with the first and the second modes of the time-dependent Nusselt number distribution were evaluated using a combined POD-tomography approach. Regions of large Nusselt number at the interface were once again seen to be associated with regions of low Nusselt number at the lower wall.

References

Andereck, C.D.; Colovas, P.W.; Degen, M.M.; Renardy, Y.Y.; (1998) Instabilities in two-layer Rayleigh-Benard convection: overview and outlook, *International Journal of Engineering Science* 36, pp. 1451-1470.

Gebhart, B.; Jaluria, Y.; Mahajan, R.; Sammakia, B.; (1988) *Buoyancy induced flows and transport*, Springer-Verlag, New York.

Goldstein, R.J.; (1996) *Fluid Mechanics Measurements*, Taylor and Francis, Second Edition.

Gollub, J.P.; Benson, S.V.; (1980) Many routes to turbulent convection, J. Fluid Mechanics, 100(3), pp. 449-470.

Golovin, A.A; Nepomnyashchy A.A.; Pismen L.M.; (1995) Pattern formation in large-scale Marangoni convection deformable interface, *Physica D*, 81, pp.117-147

Herman, G.T.; (1980) *Image Reconstruction from Projections*, Academic Press, New York.

Johnson, D.; Narayanan, R.; Dauby, P.C.; (1999) The effect of air height on pattern formation in liquid-air bi-layer convection, in *FDMP: Fluid Dynamics at Interfaces,* Cambridge University Press, Cambridge, pp. 15-30.

Jollife, I.T.; (2000) *The Principal component analysis*, Springer-Verlag, New York.

Krishnamurti, R.; (1970) On the transition to turbulent convection: The transition from two to three dimensional flow, J. Fluid Mechanics, 42(2), pp. 295-307.

Lappa, M.; (2005) On the Nature and Structure of Possible Three-dimensional Steady Flows in

Closed and Open Parallelepipedic and Cubical Containers under Different Heating Conditions and Driving Forces, *FDMP: Fluid Dynamics and Material Processing*, vol.1, no.1, pp. 1-19.

Lebon, G.; Dauby P.C.; Regnie, V.C.; (2001) Role of interface deformation on Be-Ma instability, *Acta Astronautica*, vol 48, no. 5-12, pp. 617-627.

Mishra, D.; Muralidhar, K.; Munshi; P.; (1999) Interferometric Study of Rayleigh-Benard Convection at Intermediate Rayleigh Numbers, Fluid Dynamics Research, vol. 25, no. 5, pp. 231-255.

Mosaad, M.; -Nakhi, A.B.; Al-Hajeri, M.H.; (2005) Thermal Communication between Two Vertical Systems of Free and Forced Convection via Heat Conduction across a Separating Wall, *FDMP: Fluid Dynamics and Material Process-*

ing, vol.1, no.4, pp.301-313.

Natterer, F.; (1986) *The Mathematics of Computerized Tomography*, John Wiley, New York.

Prakash, A.; Yasuda, K.; Otsubo, F.; Kuwahara, K.; Doi, T.; (1997) Flow coupling mechanism in two-layer Rayleigh-Benard convection, *Experiments in Fluids*, 23, pp. 252-261.

Punjabi, S.; Muralidhar, K.; Panigrahi, P.K.; (2004) Buoyancy-driven convection in two superposed fluid layers in an octagonal cavity, *International Journal of Thermal Sciences* 43, 849-864.

Punjabi, S.; Muralidhar, K.; Panigrahi, P.K.; (2006) Influence of Layer Height on Thermal Buoyancy Convection in A System with Two Superposed Fluids Confined in A Parallelepipedic Cavity, *FDMP: Fluid Dynamics and Material Processing*, vol.2, no.2, pp.95-105.

Renardy, Y.Y.; Stoltz, C.G.; (2000) Time-dependent pattern formation for convection in two layers of immiscible fluids, *Inter. J. Multiphase Flow*, 26, pp. 1875-1889.

Settles, G.S.; *Schlieren and Shadowgraph Techniques*, Springer, New York, 2001.

Shyy, W.; Udayakumar, H.S.; Rao, M.M.; Smith, R.W.; (1996) *Computational Fluid Dynamics with Moving Boundaries,* Taylor and Francis, New York.

Velarde,M.G.; Normand, C.; (1980) Convection, Scientific American, 243(1), pp. 79-94.

Zhao, A.X.; Wagner, C.; Narayanan, R.; Friedrich, R.; (1995) Bi-layer Rayleigh-Marangoni convection: transitions in flow structures at the interface, *Proc. R. Soc. London, Ser. A,* pp. 451-487.